PAPER

Spin-polarization control of in-plane scattering in arrays of asymmetric U-shaped nanoantennas

To cite this article: Seyed M Sadeghi et al 2023 Nanotechnology 34 415201

View the article online for updates and enhancements.

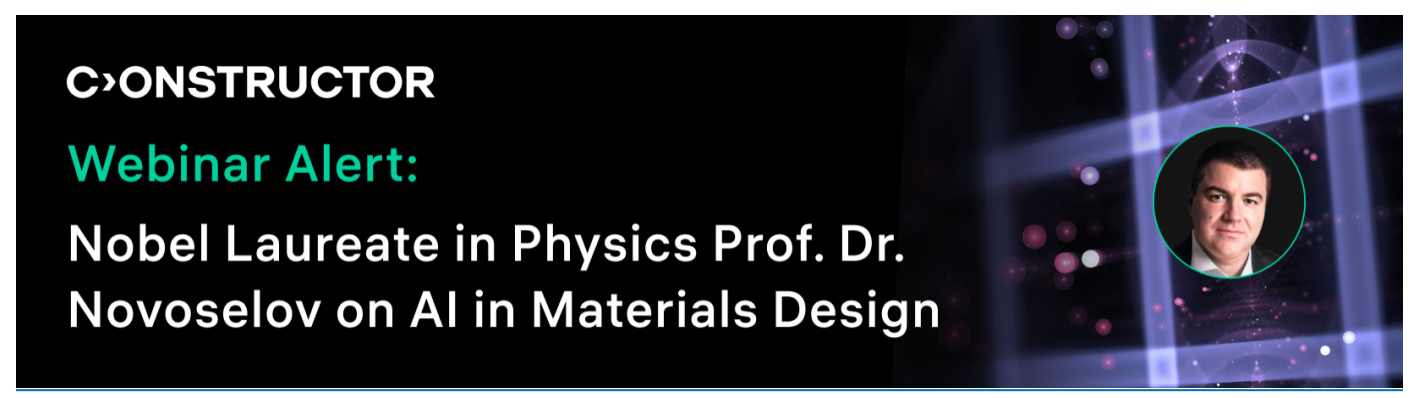
You may also like

- Multiple-resonant pad-rod nanoantennas for surface-enhanced infrared absorption spectroscopy
 Weisheng Yue, Vasyl Kravets, Mingbo Pu
- et al.

Dielectric optical nanoantennas

- Polarization-independent characteristics of the metasurfaces with the symmetrical axis's orientation angle of 45° or 135 Wei Wang, Zhongyi Guo, Lingling Ran et

Md Rabiul Hasan and Olav Gaute Hellesø



Nanotechnology 34 (2023) 415201 (10pp)

https://doi.org/10.1088/1361-6528/ace725

Spin-polarization control of in-plane scattering in arrays of asymmetric U-shaped nanoantennas

Seyed M Sadeghi, Dustin T Roberts and Rithvik R Gutha

Department of Physics and Astronomy, University of Alabama in Huntsville, Huntsville, Alabama, AL-35899, United States of America

E-mail: seyed.sadeghi@uah.edu

Received 23 March 2023, revised 3 July 2023 Accepted for publication 13 July 2023 Published 28 July 2023



Abstract

We study projection-enabled enhancement of asymmetric optical responses of plasmonic metasurfaces for photon-spin control of their far field scattering. Such a process occurs by detecting the light scattered by arrays of asymmetric U-shaped nanoantennas along their planes (in-plane scattering). The nanoantennas are considered to have relatively long bases and two unequal arms. Therefore, as their view angles along the planes of the arrays are changed, they offer an extensive range of shape and size projections, providing a wide control over the contributions of plasmonic near fields and multipolar resonances to the far field scattering of the arrays. We show that this increases the degree of the asymmetric spin-polarization responses of the arrays to circularly polarized light, offering a large amount of chirality. In particular, our results show the in-plane scattering of such metasurfaces can support opposite handedness, offering the possibility of photon spin-dependent directional control of energy routing.

Supplementary material for this article is available online

Keywords: plasmonic metasurfaces, interference processes, spin photon, polarization spin, inplane scattering, nanoantennas, multipolar plasmon resonances

1

(Some figures may appear in colour only in the online journal)

1. Introduction

Plasmonic metasurfaces include two-dimensional arrays of metallic nanoantennas capable of controlling optical phase and near field properties in sub-wavelength scales [1, 2]. Such features can be tailored by varying the sizes and shapes of the nanoantennas, and considering different material structures. The wide range applications of plasmonic metasurfaces include novel optical devices [3–7], biosensors [8, 9], and metalenses [10]. They also include enhancement of nonlinear effects [11], generation of chiral materials [11–13], negative refractive index [8, 9], and superchiral polarimetry [14]. Plasmonic metasurfaces are also used to investigate planar chirality wherein the differences in the interaction of right and left circularly polarized light (RCP and LCP) is utilized to generate different forms of near field interaction in ultrathin layers of materials [15–20]. Such planar chiral structures

allow plasmonic dichroism without a need for close coupling with chiral molecules [21–23], radiative coupling with chiral isotropic medium [24], orbital hybridization [25], or dipoledipole interactions between chiral molecules and plasmonic nanoparticles [26]. Additionally, metasurfaces based on opposite-chirality-coexisted meta-atoms is shown to support four independent circular polarization information channels, useful for polarization and frequency multiplexing [27].

In two-dimensional chiral structures control of plasmonic resonances of nanoantennas via structural optimization plays a key role [28, 29]. Along this, periodic arrays of V-shaped [3, 6, 7, 30], L-shaped [31–34], and gammadion-shaped nanoantennas [19], have been investigated. Addiotionally, perforated S-shaped holes [35], and Au planar heptamers have also been explored [36]. In these cases the presence of the substrates and/or variations of shapes along the light propagation axis, which break the symmetry, effectively

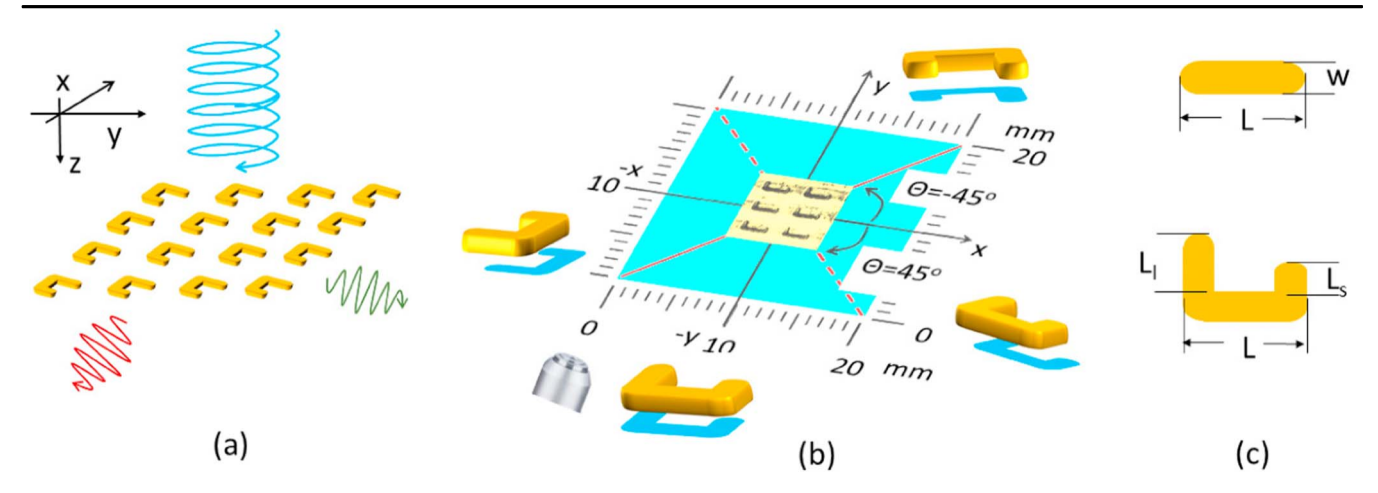


Figure 1. (a) Schematic of the asymmetric U-shaped nanoantenna array and its side-scattering. (b) Projections of the asymmetric U-shaped nanoantennas as viewed from four sides of the array at given angles of view. The arrays are fabricated on square glass substrates with 20 mm sides. An objective scans the in-plane scattering from each side of the substrate within 0–20 mm range. (c) Scales and side denominations of the NR and U-shaped nanoantennas.

transforms these structures into quasi three dimensional arrays. Therefore, the incident light reaching the arrays from opposite directions experiences different structural features. Recent reports have shown that the chiral near field distributions of two-dimensional plasmonic metastructures can be detected using the fluorescence properties of achiral quantum emitters [37, 38].

In a recent report we studied in-plane far field scattering (side scattering) of metasurfaces consisting of periodic arrays of plasmonic bracket structures (Additional demonstrating a transition between two super-cell states associated with such structures [39]. In-plane scattering of arrays of flat nanorods (NRs) has also been used to demonstrate application of surface lattice resonances for an optical polarization switching process for far field scattering with high extinction ratio [40]. Previous reports have also extensively focused on symmetric U-shaped nanoantennas (split ring resonantors) for enhancement of nonlinear effects and chirality [41], and enhancement of second harmonic generation [42, 43]. Recent reports have also shown that when a quantum dot is coupled to such a nanoantenna, the polarization state of its emission can be controlled, leading to chiral light of opposite handedness [44].

In this paper, we investigate the photon-spin control of in-plane far-field scattering (in-plane scattering) in plasmonic metasurfaces consisting of arrays of asymmetric U-shaped nanoantennas (figure 1(a)). We show that, since such a scattering is detected along the planes of the metasurfaces, the positions and angles of view of the nanoantennas can offer projection-enabled enhancement of asymmetric optical responses of the arrays. As schematically shown in figure 1(b), such a process is based on the fact that, because of the asymmetry of the nanoantennas, with variations of the angle of sideview, the size and shape projections of the U-shaped nanoantennas can become dramatically different. The asymmetry of the nanoantennas not only affects their size and shape projections but also enhances their multipolar resonances, leading to the introduction of additional pathways for interference processes that influence the in-plane

scattering [45]. Consequently, extensive photon-spin asymmetric features are observed in such scattering, which are not observed in the front or back scattering of the arrays along the z-axis (figure 1(a)).

We show that a prime impact of the projection-enabled enhancement of asymmetry in the nanoantennas arrays considered in this paper is formation of significant amount of directional chirality. This highlights the effects of the two unequal arms of the nanoantennas in generation of polarization-dependent near fields and photon-spin dependent phase properties. Mapping of the in-plane scattering around the edges of the substrates supporting the asymmetric U-shaped nanoantenna arrays (figure 1(b)) shows that the scattering detected from each side offers different photon-spin responses. In other words, the scattering detected along the x-axis (figure 1(b)) shows a higher efficiency for RCP, while on the side of the longer arms (the y-axis) the scattering seems to be more dominated by LCP. This suggests a directional chiral scattering with opposite handedness, highlighting photon spin-dependent routing of the scattered light. These results offer a unique perspective of how asymmetry of meta-atoms can be employed to control the coherent balance of contributions of the multipolar plasmonic resonances, leading to chiral properties.

2. Methodology

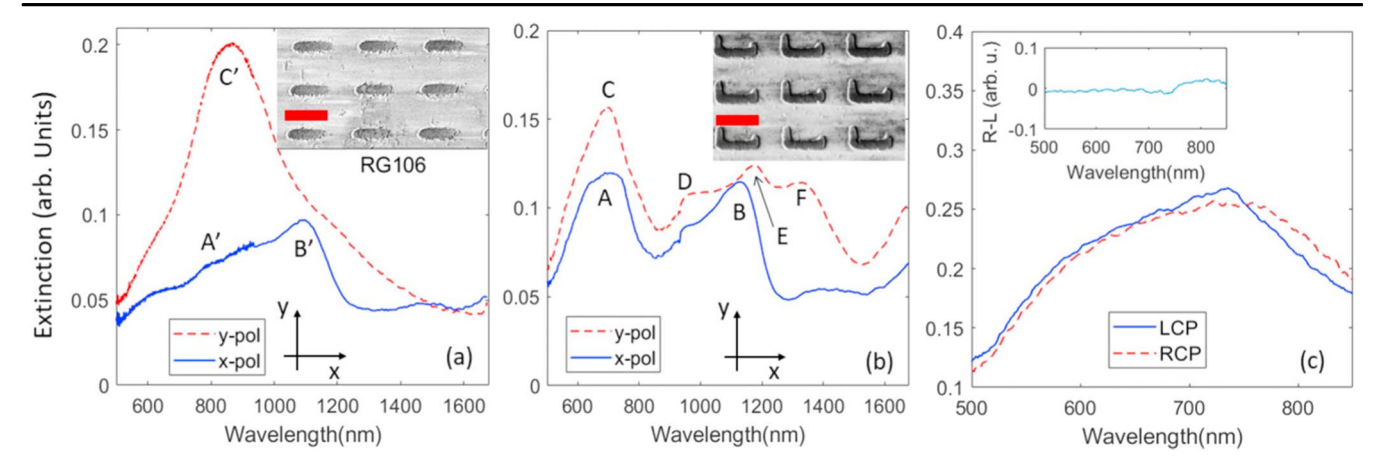


Figure 2. Extinction spectra of the NR arrays (a), and the asymmetric U-shaped nanoantenna arrays (b), for x-pol (solid lines) and y-pol (dashed lines). (c) shows the extinction spectra of the U-shaped nanoantenna array for an incident light with RCP (dashed line) and LCP (solid line). The insets in (a) and (b) refer to the SEM images of the corresponding samples, and in (c) to the difference between RCP and LCP extinction spectra.

the lattice constants along x-axis (a_x) and y-axis (a_y) were 1.5 and 1 μ m, respectively.

The extinction spectra of the samples when the incident light reaches the samples at normal angle with polarization along the x-axis (x-pol) or y-axis (y-pol) are shown in figures 2(a) and (b). The results show that for x-pol (solid lines) samples 1 and 2 have a peak with similar wavelengths (peaks B' and B). These peaks can be associated with the longitudinal modes of the NRs and the bases of asymmetric U-shaped nanoantennas with lengths L (figure 1(c)). For the same incident light polarization, however, the asymmetric U-shaped nanoantenna arrays (sample 1) have a prominent peak around 693 nm (peak A). This peak can be associated with the transverse modes of the arms. One expects that the wavelengths of these modes to be close to each other. In the case of NR array, however, at about 800 nm we can only see a small kink (kink A').

For y-pol (dashed lines) the NR arrays mostly support a broad peak at about 830 nm (peak C'). The extinction spectrum of arrays of asymmetric U-shaped nanoantennas, however, is quite different. Here in addition to a peak at similar wavelength as that of peak A (peak C), we can see three extra peaks about 1000 (peak D), 1150 (peak E), and 1300 nm (peak F). Note that peak C' in may be associated with surface lattice resonances of the NR arrays [46–48].

To analyze the impact of phase and multipolar modes dictated by the structural features (asymmetry properties) of the nanoantenna arrays, we spectrally analyze the in-plane scattering of samples 1 and 2. For this we used an optical setup consisting of a broad white light source, a polarizer (P1), and a microscope objective (objective 1) to focus the light on the samples with a given polarization (figure S1, supporting information). The scattered light was then collected by a second microscope objective (objective 2). As schematically shown in figure 1(b), objective 2 was moved along the edges of the substrates of the arrays, mapping the in-plane scattering. The range of movement of this objective was between 0 and 20 mm, i.e. the whole length of the sides of the substrates. The angle of polarization of incident light

(θ) was measured with respect to the x-axis (figure S1). The optical setup used to study chiral in-plane scattering was similar, but with some differences. Here, as shown in figure S2, we used a 780 nm laser beam combined with a quarter-wavelength to generate RCP and LCP beams with the same intensities. The power of the laser beam was then collected via an objective (objective 2) and measured with a power-meter.

3. Spectral in-plane scattering

The results of the in-plane scattering of the NR arrays when it was detected along the x-axis and $\theta = 0^{\circ}$ (x-pol) and 90° (ypol) are shown in figures 3(a) and (b), respectively. The results show the amount scattering is significantly more for ypol (figure 3(b)). This can be associated with the fact that for such a polarization the plasmonic dipoles of the NRs are excited more efficiently within the range of our detector sensitivity. In both cases, however, we can see scattering mostly occurs at wavelength longer than 750 nm. Detection of the light scattering along the y-axis, however, offers a different perspective (figures 3(c) and (d)). One crucial difference between this case and those shown in figures 3(a) and (b) is their spectral features. In fact when detection occurs along the y-axis, the scattered light has a spectral bandwidth reaching 550 nm. Additionally, the results suggest that the scattered light is more concentrated around 750 and 1100 nm.

The results for the case of asymmetric U-shaped nanoantenna arrays are shown in figures 3(a')-(d'). These results show significant differences compared to the case of the NR arrays, indicating the profound impact of the nanoantennas arms and size/shape projections on the spectra and intensity of in-plane scattering. Figure 3(a') shows that for x-pol and when the scattering is detected along the x-axis, the scattered light is more spectrally localized at about 710 and 910 nm. For y-pol, however, the scattering concentrates in the infrared range (2920 nm) with much higher efficiency (figure 3(b')). Figures 3(c') and (d') also show significant

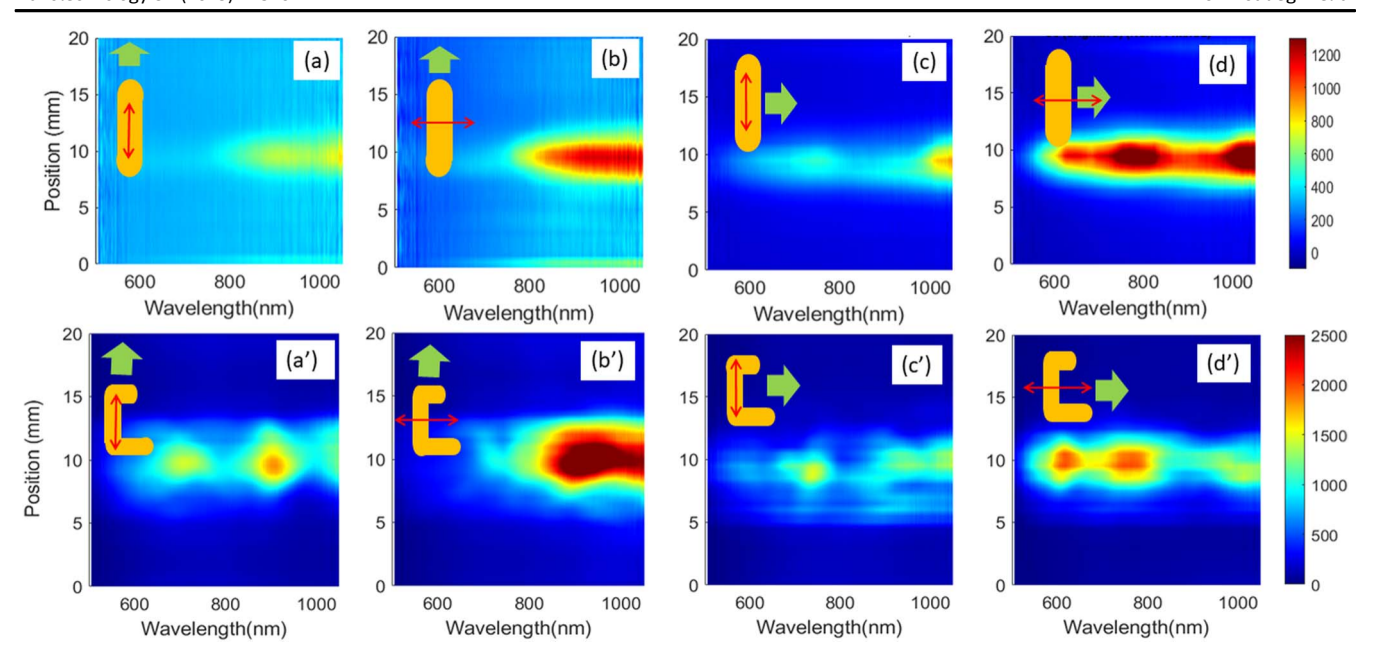


Figure 3. (a) and (b): The in-plane scattering for the NR arrays as a function of position when it was measured along the x-axis and the incident light has x-pol and y-pol, respectively. (c) and (d) are as (a) and (b) but the scattering was measured along the y-axis. (a')–(d') are as (a)–(d) but for the asymmetric U-shaped nanoantenna arrays. The inset in each figure shows the direction of detection of scattered light (green arrows) and the axis of the incident light polarization (double-sided red arrows). The numbers on the scale bars refer to the detected scattering counts.

changes in the scattering when it was detected along the y-axis. Comparison of the results presented in figures 3(c) with (c') shows that for x-pol the impact of the unequal arms of the asymmetric U-shaped nanoantennas includes some scattering around 750, 950, and 1100 nm with relatively low counts. For the case of y-pol, however, as comparison of figures 3(d) and (d') shows, the extra arms of the asymmetric U-shaped nanoatennas have profound impact on the scattering spectrum. In fact here the scattering is more concentrated at \$\mathbb{D}600\$ and \$\mathbb{D}780\$ nm. Note that for better clarity the color coded scales of the scattering counts of the NR array are considered between 0 and 1300. In the case of asymmetric nanoantenna array, however, the bar is between 0 and 2500, indicating more efficient scattering by such an array.

4. Photon-spin control of in-plane scattering

The core aspect of this paper is investigation of enhanced photon-spin responses of asymmetric U-shaped nanoantennas by expanding the way plasmonic multipolar resonances and phase can contribute to the scattering processes. To study this we used the optical setup shown in figure S2. Figure 4 shows the results for the power collected by objective 2 as it moved along the edges of the substrate containing the asymmetry U-shaped nanoantennas. The results show the prominent differences between the scattering of the laser field for RCP (dashed lines) and LCP cases (solid lines). When the scattered laser beam is detected along the x-axis, the scattered intensity for RCP is about two times of that of LCP (figure 4(a)). The inset in this figure shows the results for $I_{\rm CD}$ = $I_{\rm RCP}$ – $I_{\rm LCP}$, with a peak amplitude of about 35 nW ($I_{\rm RCP}$ and $I_{\rm LCP}$ are the

intensities associated with the dashed and solid lines in figure 4, respectively).

Detection of the scattered laser field along the -y-axis, however, shows the opposite case, indicating a more intense scattering with LCP (figure 4(b)). The inset here shows a $I_{CD} = -25$ nW. Such a switching from positive to negative I_{CD} is an indication of how the arms of the nanoantennas play a key role on the nature of near and far fields of the arrays. The results when the scattered laser field was detected along the -x-axis also offer $I_{CD} = -35$ nW (figure 4(c)). Comparison of these results with those in figure 4(a) shows how the lengths of the arms influence the polarization-dependent scattering process. In other words, along the x-axis, i.e. when we face the shorter arm, the scattering intensity for RCP is higher than LCP. When detection occurs along the same axis but facing the longer arm, however, the scattering is more for LCP (figure 4(c)). This highlights a photon spin-dependent routing process, wherein the handedness of the incident light polarization decides the direction of the scattering.

Alternatively, we can explore the efficiency of these processes by defining an in-plane scattering anisotropy factor (g) as [49]:

$$g(r) = \frac{A_{-}(r) - A_{+}(r)}{\hat{A}(r)}.$$
 (1)

Here $A_+(r)$ and $A_-(r)$ refer to the in-plane scattering power associated RCP and LCP, respectively. r = x for is detection along the y-axis and r = y for detection along the x-axis. $\hat{A}(r)$ is the their average, given by:

$$\hat{A}(r) = \frac{A_{+}(r) + A_{-}(r)}{2}.$$
 (2)

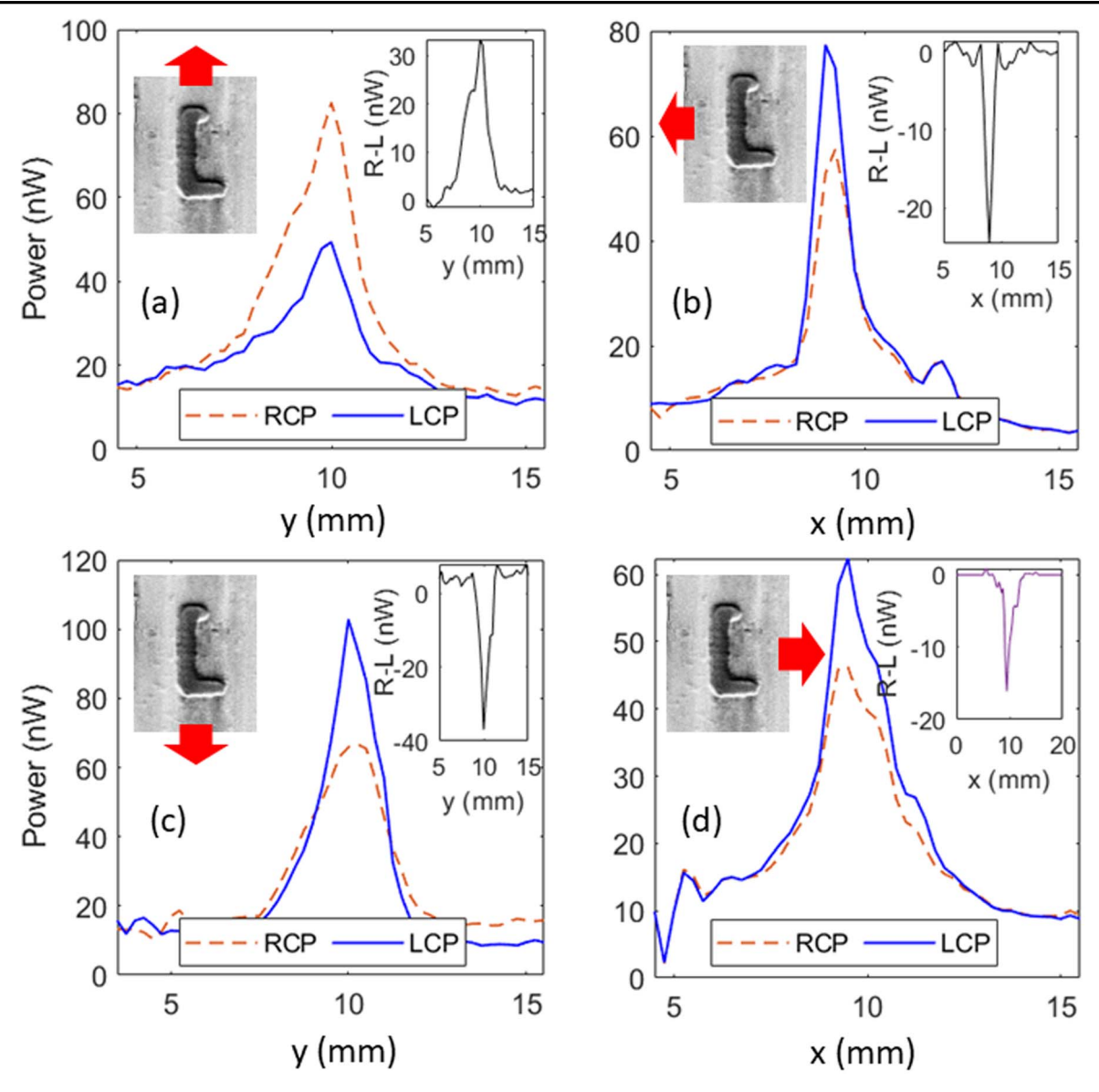


Figure 4. In-plane scattering of the asymmetric U-shaped nanoantenna arrays when the incident laser beam is right (dashed lines) and left (solid lines) circularly polarized. The insets shows the SEM images of a unit of the array and the directions of detection of the in-plane scattering (red arrows). In (a) light is detected along the x-axis, in (b) along the -y-axis, in (c) along the -x-axis, and in (d) along the y-axis. The right insets shows the difference between RCP and LCP scattered light.

The results shown in the supporting information section (figure S3(a)) indicate a maximum value of g of about 0.5 for the results shown in figure 4(a). On the other hand, for the case of figure 4(c), i.e. detection along the -x-axis, g has a minimum of about -0.4 (figure S3(c)).

To further discuss the photon-spin control via projectionenabled asymmetry, we used an achromatic quarter-wave plate with effective range from 500 to 800 nm to study the extinction spectra and in-plane scattering sample 1 for LCP and RCP when the incident light was a white light source. The results for the extinction spectra are shown in figure 2(c). These results show very small variations in the spectra as the incident light polarization changes from RCP to LCP. In fact at 750 nm the percentage of variations is found about 4%, which is within the systematic errors of our system. This shows, when viewed from the front, the asymmetry of the U-shaped nanoantennas studied in this paper does not amount to any significant chirality. Note that around 800 nm, the efficiency of quarter wavelength plate was reduced, therefore, this region was ignored.

The in-plane scattering, however, offers a different scenario. To see this, we carried out spectral in-plane spectroscopy similar to that in figure 3, but instead of linearly polarized light we used a white light source with LCP and RCP. The results presented in figure 5 show that when scattering was detected along x-axis, LCP (figure 5(a)) and RCP (figure 5(b)) offer different results. This indicates high spin-photon selectivity caused by harvesting the asymmetry of the nanoantennas when they are viewed from the side. Figure 5(c) shows the difference between the counts associated with LCP and RCP. Considering these results, at 750 nm we found the percentage of variations of the RCP and LCP counts about

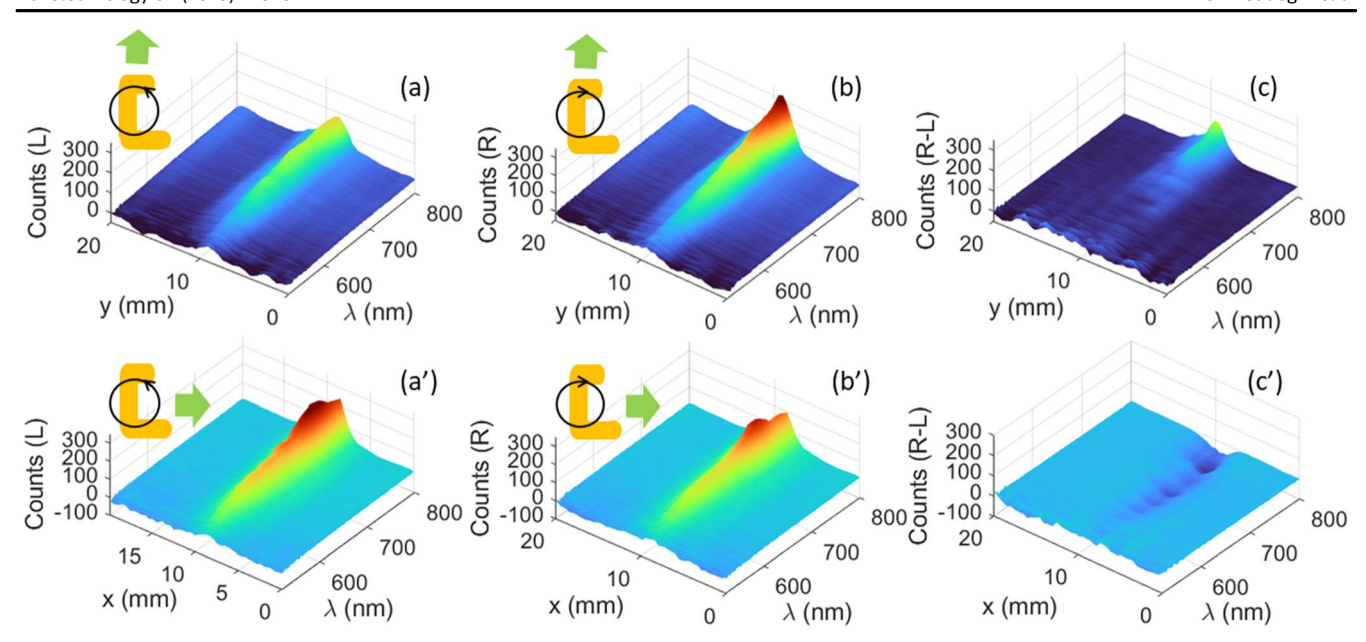


Figure 5. The x-axis in-plane scattering of the asymmetric U-shaped nanoantenna arrays as a function of position when the incident light has LCP (a) and RCP (b). (a') and (b') are as (a) and (b) but the scattering was measured along the y-axis (green arrows). (c) and (c') show the differences between LCP and RCP when scattering detected along the x-and y-axes, respectively.

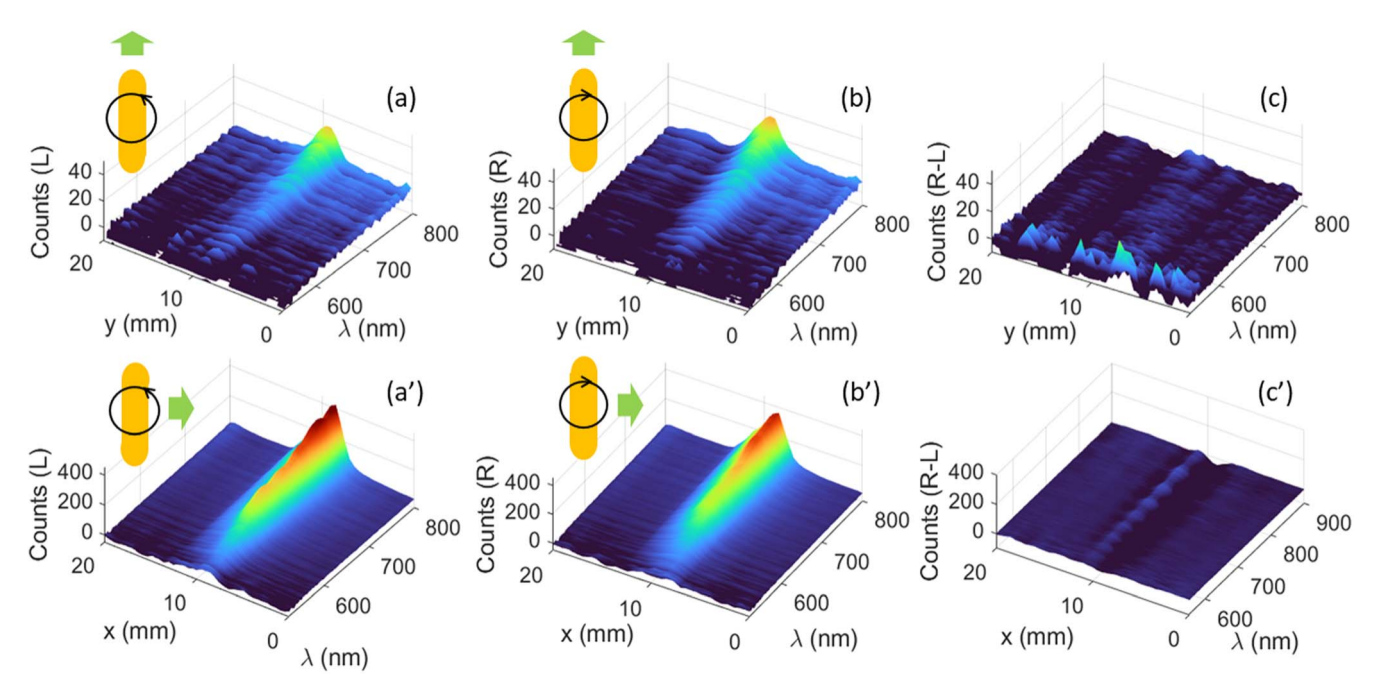


Figure 6. The x-axis in-plane scattering of the NR arrays as a function of position for incident light with LCP (a) and RCP (b). (a') and (b') are as (a) and (b) but the scattering was measured along the y-axis. (c) And (c') show the differences between LCP and RCP when scattering detected along x-axis and y-axis, respectively.

40%, which is about one order magnitude higher than that seen in the case extinction spectra (figure 2(c)). For the case when scattering was detected along y-axis, however, we observed a less level of chirality (figures 5(a')-(c')). It is obvious, however, that here the scattering counts via LCP is more than that RCP, as also indicated in figure 5(c'). The contrast between these results and those in figures 5(a) and (b) can be attributed to the fact that these two cases correspond to different paths of in-plane scattering detection. Consequently,

they depend on different viewing angles and side view projections of the nanoantennas, which ultimately affect the chiral response. Figure 6 shows the results for the case of the NR arrays. These results suggest that the differences between LCP and RCP when the scattering detected along the x-axis (figures 6(a)–(c)) and y-axis (figures 6(a')–(c')) are insignificant. Comparing these results with those presented in figures 3(a)–(d), however, shows the contrast of scattering for NR arrays for linearly and circularly polarized light. When the

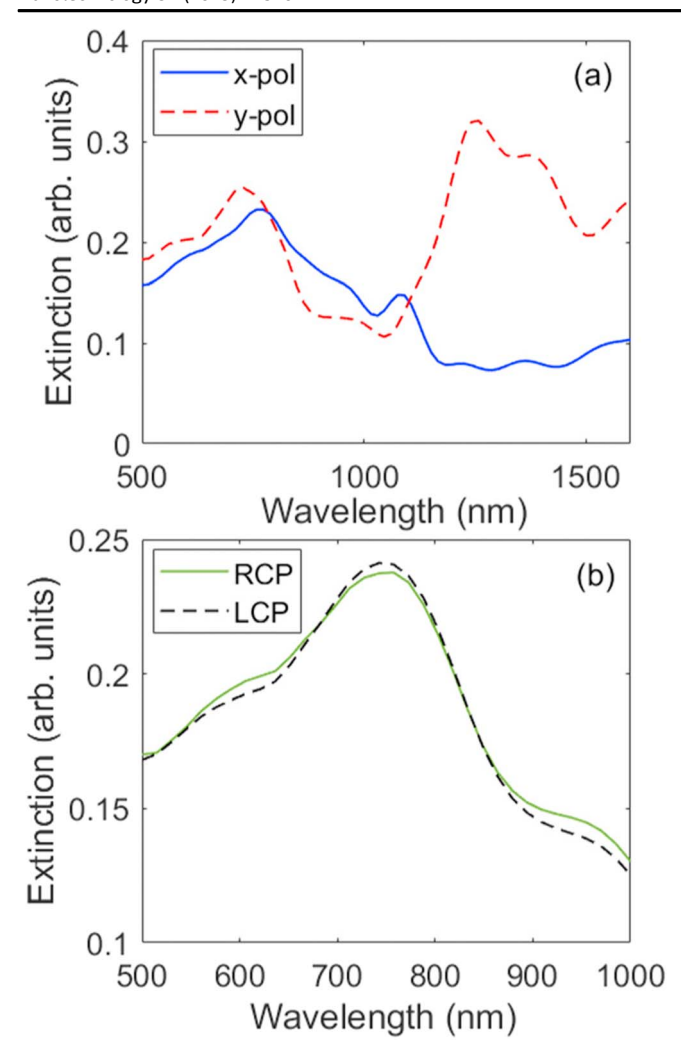


Figure 7. (a) Simulation results for extinction spectra of the asymmetric U-shaped nanoantennas when the incident light is linearly polarized along the x-axis (solid line) and y-axis (dashed line). (b) Simulation results when the incident light is RCP (solid line) and LCP (dashed line). Here the substrate is considered to be glass and the superstrate is air.

scattering detected along x-axis, for example, the results of these two cases seem to be similar spectrally. However, for scattering detected along the y-axis, these two cases lead to different spectral outcomes. In fact for the case of circularly polarized light the scattering intensity is mostly increased with wavelength monotonously (figures 6(a') and (b')). In the case of linear polarization, however, the scattering counts are mostly concentrated at 780 and 1000 nm. This can be associated with the fact that the scattering of NR arrays is solely associated with single NR scattering. Rather, the contributions of other NRs lead to a collective response.

To analyze the plasmonic modes of the asymmetric U-shaped nanoantenna array, we analyze their mode properties using finite difference time domain (FDTD) method. For this, using the Device Multiphysics Simulation Suite of Lumerical software (2020a version), we considered a structural file consisting of a Au asymmetric U-shaped nanoantenna with similar dimensions to those in figure 1(c). Such a nanoantenna had periodic boundary conditions along the x- and y-axes and the

light was reaching from the top (figure S4). Figure 7(a) shows the results of the simulation for the extinction spectra for x-pol (solid line) and y-pol (dashed line). Comparing with the experimental results shown in figure 2(b), the simulation results show the main features, although lack of inclusion of edge roundness, shapes and size fluctuations have led to some discrepancies. Figure 7(b) show that results when the incident light was considered to be RCP (solid line) and LCP (dashed line). Again, here the results seem to be in good match with those presented in figure 2(c). These results emphasize the fact that for the range of wavelength considered considered in this figure, the impact of photon spin in the extinction spectra of sample 1 is insignificant.

Figures S5(a)–(f) show the modal field enhancement factors, defined as the field intensity in the presence of the nanoantennas arrays to that in their absence, for y-pol at different wavelengths. These results suggest the peak at about 727 nm has a multipolar character along the longer arms of the nanoantennas (figure S5(b)). At 1000 nm this is replaced with a transverse mode for the base of the nanoantennas (figure S5(c)). At 1242, 1393, and 1621 nm, as seen in figures S5(d)–(f), the dominant asymmetric modes of the nanoantennas become quite evident. Distinct asymmetric modal features can also be seen in the case of x-pol, as shown in figures S5(a')–(c') for 757, 1075, and 1727 nm, respectively.

The results of simulation for modal field enhancement factors when the incident light is RCP and LCP are shown in figure 8. This figure provides clear contrasts in the mode profiles associated with these polarization states at 606 nm ((a) and (a')), 742 ((b) and (b')), and 969 nm ((c) and (c')). The results show how the combined impact of asymmetry of U-shaped nanoantennas and circularly polarized light on the plasmonic mode enhancement factors. The outcome suggest dramatically different near fields, particularly at 742 and 969 nm. Such a pronounced chiral field, however, does not have significant impact in the far field when detected along the z-axis, as suggested by figures 2(c) and 7(b).

Note that previous reports have shown that in-plane scattering in arrays of nanoantennas can be influenced by the interference processes between different scattering components associated with the plamson modes of the nanoantennas [44, 45, 50, 51]. As shown in [45], such processes allow control of directions and wave-fronts of the scattered light. In the case of asymmetric U-shaped nanoantennas considered in this paper, different angles of view (figure 1(b)) is expected to project different phase and paths of interference processes. Additionally the high degree of structural asymmetric allow resonance excitations of different plasmonic modes at a given wavelengths. Therefore, here we deal with phase interference processes of multipolar processes that can are controlled by the angles of view.

Note that the results of this paper introduced chirality to metasurfaces that, based on transmission-based measurements, would otherwise be considered nearly achiral. This opens up new avenues for the development of chiral structures. Additionally, since the systems studied in this paper employed an inplane scattering configuration, they provide a significantly larger footprint for the interaction of light with nanoantennas compared

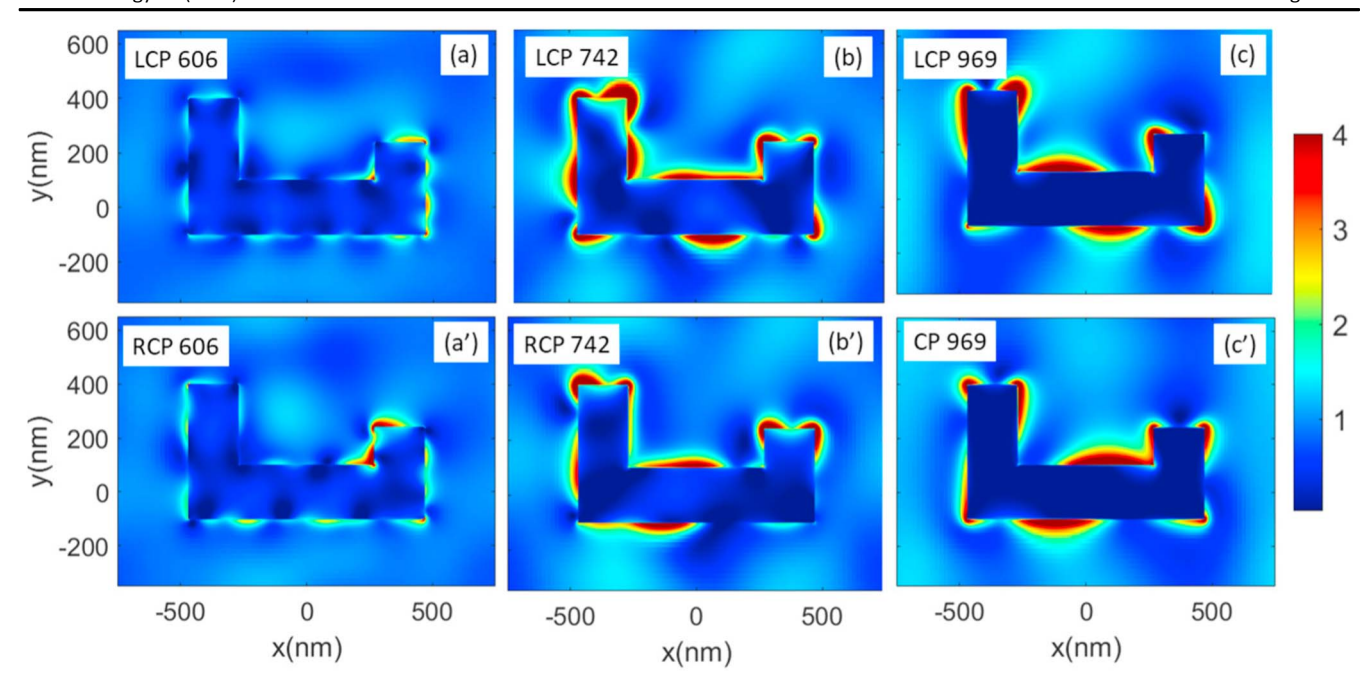


Figure 8. Simulation results for the modal field enhancement factors in the x-y plane for 606, 742, and 969 nm when the incident beam is LCP ((a)-(c)) and RCP ((a')-(c')). The vertical color bar refers to the range of the field enhancement factor. The x-y plane passes through the middle of the height of the nanoantenneas, i.e. 20 nm from the substrate.

to transmission-based systems. This feature holds the potential to offer significant advantages in sensor applications and devices, including lasers and in-plane optical filters [52, 53].

5. Conclusions

We studied enhancement of photon-spin dependency of the far field optical responses of plasmonic metasurfaces consisting of periodic arrays of asymmetric U-shaped Au nanoantennas. Such a process happened when the far field scattering was detected along the planes of the arrays (inplane scattering). Our results showed that this can lead to extensive chiral optical responses, as the size and shape projections of nanoantennas were changed dramatically with position and angle of view, when the arrays were viewed from their sides. Combination of this with the impact of circularly polarized light offered a unique technique wherein far field scattering can effectively carry the effects associated with the photon spin dependent near fields and the interference processes associated with multipolar plasmon resonances. Our results showed that the large degrees of structural asymmetry of the nanoantennas studied in this paper supports enhancement of interference processes at different wavelengths, leading to significant different side-dependent in-plane scattering. The outcomes offerred extended regime of photon-spin control of scattering and its directional control.

Acknowledgments

This research was supported by US National Science Foundation under grant no. ECCS-1917544.

Data availability statement

All data that support the findings of this study are included within the article (and any supplementary files).

ORCID iDs

Seyed M Sadeghi https://orcid.org/0000-0002-5043-5032

References

- [1] Gansel J K, Thiel M, Rill M S, Decker M, Bade K, Saile V, von Freymann G, Linden S and Wegener M 2009 Gold helix photonic metamaterial as broadband circular polarizer Science 325 1513-5
- [2] Shimotsuma Y, Kazansky P G, Qiu J and Hirao K 2003 Selforganized nanogratings in glass irradiated by ultrashort light pulses Phys. Rev. Lett. 91 247405
- [3] Kildishev A V, Boltasseva A and Shalaev V M 2013 Planar photonics with metasurfaces Science 339 1232009
- [4] Solntsev A S, Agarwal G S and Kivshar Y S 2021 Metasurfaces for quantum photonics Nat. Photon. 15 327–36
- [5] Georgi P, Massaro M, Luo K H, Sain B, Montaut N, Herrmann H, Weiss T, Li G, Silberhorn C and Zentgraf T 2019 Metasurface interferometry toward quantum sensors Light: Sci. Appl. 8 1–7
- [6] Chen H T, Taylor A J and Yu N 2016 A review of metasurfaces: physics and applications Rep. Prog. Phys. 79 076401
- [7] Kats M A, Genevet P, Aoust G, Yu N, Blanchard R, Aieta F, Gaburro Z and Capasso F 2012 Giant birefringence in optical antenna arrays with widely tailorable optical anisotropy Proc. Natl. Acad. Sci. 109 12364–8

- [8] Zhang S, Park Y S, Li J, Lu X, Zhang W and Zhang X 2009 Negative refractive index in chiral metamaterials Phys. Rev. Lett. 102 023901
- [9] Jakšić Z, Vuković S, Matovic J and Tanasković D 2010
 Negative refractive index metasurfaces for enhanced biosensing Materials 4 1-36
- [10] Khorasaninejad M, Chen W, Zhu A, Oh J, Devlin R, Rousso D and Capasso F 2016 Multispectral chiral imaging with a metalens Nano Lett. 16 4595–600
- [11] O'Brien K, Suchowski H, Rho J, Salandrino A, Kante B, Yin X and Zhang X 2015 Predicting nonlinear properties of metamaterials from the linear response Nat. Mater. 14 379–83
- [12] Auguié B, Alonso-Gómez J L, Guerrero-Martínez A and Liz-Marzán L M 2011 Fingers crossed: optical activity of a chiral dimer of plasmonic nanorods J. Phys. Chem. Lett. 2 846-51
- [13] Decker M, Zhao R, Soukoulis C, Linden S and Wegener M 2010 Twisted split-ring-resonator photonic metamaterial with huge optical activity Opt. Lett. 35 1593-5
- [14] Tullius R, Karimullah A S, Rodier M, Fitzpatrick B, Gadegaard N, Barron L D, Rotello V M, Cooke G, Lapthorn A and Kadodwala M 2015 Superchiral spectroscopy: detection of protein higher order hierarchical structure with chiral plasmonic nanostructures J. Am. Chem. Soc. 137 8380-3
- [15] Hecht L and Barron L D 1994 Rayleigh and raman optical activity from chiral surfaces Chem. Phys. Lett. 225 525–30
- [16] Poulikakos L V, Thureja P, Stollmann A, De Leo E and Norris D J 2018 Chiral light design and detection inspired by optical antenna theory Nano Lett. 18 4633–40
- [17] Cotrufo M, Osorio C I and Koenderink A F 2016 Spindependent emission from arrays of planar chiral nanoantennas due to lattice and localized plasmon resonances ACS Nano 10 3389–97
- [18] Eftekhari F and Davis T 2012 Strong chiral optical response from planar arrays of subwavelength metallic structures supporting surface plasmon resonances Phys. Rev. B 86 075428
- [19] Kuwata-Gonokami M, Saito N, Ino Y, Kauranen M, Jefimovs K, Vallius T, Turunen J and Svirko Y 2005 Giant optical activity in quasi-two-dimensional planar nanostructures Phys. Rev. Lett. 95 227401
- [20] Le K Q, Hashiyada S, Kondo M and Okamoto H 2018 Circularly polarized photoluminescence from achiral dye molecules induced by plasmonic two-dimensional chiral nanostructures J. Phys. Chem. C 122 24924–32
- [21] Schaaff T G and Whetten R L 2000 Giant gold- glutathione cluster compounds: intense optical activity in metal-based transitions J. Phys. Chem. B 104 2630-41
- [22] Levi-Belenkova T, Govorov A O and Markovich G 2016 Orientation-sensitive peptide-induced plasmonic circular dichroism in silver nanocubes J. Phys. Chem. C 120 12751-6
- [23] Slocik J M, Govorov A O and Naik R R 2011 Plasmonic circular dichroism of peptide-functionalized gold nanoparticles Nano Lett. 11 701–5
- [24] Abdulrahman N A, Fan Z, Tonooka T, Kelly S M, Gadegaard N, Hendry E, Govorov A O and Kadodwala M 2012 Induced chirality through electromagnetic coupling between chiral molecular layers and plasmonic nanostructures Nano Lett. 12 977–83
- [25] Xia Y, Zhou Y and Tang Z 2011 Chiral inorganic nanoparticles: origin, optical properties and bioapplications Nanoscale 3 1374–82
- [26] Govorov A O, Gun'ko Y K, Slocik J M, Gérard V A, Fan Z and Naik R R 2011 Chiral nanoparticle assemblies: circular dichroism, plasmonic interactions, and exciton effects J. Mater. Chem. 21 16806–18

- [27] Gou Y, Ma H F, Sun S, Zhang T Y, Wu L W, Wang Z X, Zheng S and Cui T J 2023 Non-interleaved four-channel metasurfaces for simultaneous printing and holographic imaging Small Structures 2300054
- [28] Liu L, Zhang X, Kenney M, Su X, Xu N, Ouyang C, Shi Y, Han J, Zhang W and Zhang S 2014 Broadband metasurfaces with simultaneous control of phase and amplitude Adv. Mater. 26 5031–6
- [29] Ashalley E, Ma C P, Zhu Y S, Xu H X, Yu P and Wang Z M 2021 Recent progress in chiral absorptive metamaterials J. Electron. Sci. Technol. 19 100098
- [30] Yu N, Aieta F, Genevet P, Kats M A, Gaburro Z and Capasso F 2012 A broadband, background-free quarter-wave plate based on plasmonic metasurfaces Nano Lett. 12 6328–33
- [31] Wang Y, Deng J, Wang G, Fu T, Qu Y and Zhang Z 2016 Plasmonic chirality of l-shaped nanostructure composed of two slices with different thickness Opt. Express 24 2307–17
- [32] Ullah H, Abudukelimu A, Qu Y, Bai Y, Aba T and Zhang Z 2020 Giant circular dichroism of chiral 1-shaped nanostructure coupled with achiral nanorod: anomalous behavior of multipolar and dipolar resonant modes Nanotechnology 31 275205
- [33] Cameron R P and Barnett S M 2014 Optical activity in the scattering of structured light Phys. Chem. Chem. Phys. 16 25819–29
- [34] Ye W, Yuan X, Guo C, Zhang J, Yang B and Zhang S 2017 Large chiroptical effects in planar chiral metamaterials Phys. Rev. Appl. 7 054003
- [35] Arteaga O, Sancho-Parramon J, Nichols S, Maoz B M, Canillas A, Bosch S, Markovich G and Kahr B 2016 Relation between 2d/3d chirality and the appearance of chiroptical effects in real nanostructures Opt. Express 24 2242–52
- [36] Zu S, Bao Y and Fang Z 2016 Planar plasmonic chiral nanostructures Nanoscale 8 3900-5
- [37] Meinzer N, Hendry E and Barnes W L 2013 Probing the chiral nature of electromagnetic fields surrounding plasmonic nanostructures Phys. Rev. B 88 041407
- [38] Poulikakos L V, Gutsche P, McPeak K M, Burger S, Niegemann J, Hafner C and Norris D J 2016 Optical chirality flux as a useful far-field probe of chiral near fields ACS Photon. 3 1619–25
- [39] Sadeghi S M, Roberts D T, Gutha R R, Allen S and Sharp C 2022 Polarization optical switching between supercell states of plasmonic metasurfaces Phys. Rev. A 106 063518
- [40] Sadeghi S M, Gutha R R, Ramsay S, Roberts D and Sharp C 2022 Polarization optical switching based on the molding of coherent light scattering via surface lattice resonances Mater. Today Nano 18 100190
- [41] Huang Z, Yao K, Su G, Ma W, Li L, Liu Y, Zhan P and Wang Z 2018 Graphene-metal hybrid metamaterials for strong and tunable circular dichroism generation Opt. Lett. 43 2636–9
- [42] Keren-Zur S, Avayu O, Michaeli L and Ellenbogen T 2016 Nonlinear beam shaping with plasmonic metasurfaces ACS Photon. 3 117–23
- [43] Michaeli L, Keren-Zur S, Avayu O, Suchowski H and Ellenbogen T 2017 Nonlinear surface lattice resonance in plasmonic nanoparticle arrays Phys. Rev. Lett. 118 243904
- [44] Kruk S S, Decker M, Staude I, Schlecht S, Greppmair M, Neshev D N and Kivshar Y S 2014 Spin-polarized photon emission by resonant multipolar nanoantennas ACS Photon. 1 1218–23
- [45] Lin J, Mueller J B, Wang Q, Yuan G, Antoniou N, Yuan X C and Capasso F 2013 Polarization-controlled tunable directional coupling of surface plasmon polaritons Science 340 331-4
- [46] Sadeghi S M, Wing W J and Campbell Q 2016 Tunable plasmonic-lattice mode sensors with ultrahigh sensitivities and figure-of-merits J. Appl. Phys. 119 244503

- [47] Kravets V G, Kabashin A V, Barnes W L and Grigorenko A N 2018 Plasmonic surface lattice resonances: a review of properties and applications Chem. Rev. 118 5912–51
- [48] Rodriguez S R K, Schaafsma M C, Berrier A and Rivas J G 2012 Collective resonances in plasmonic crystals: Size matters Physica B 407 4081–5
- [49] Kong X T, Khosravi Khorashad L, Wang Z and Govorov A O 2018 Photothermal circular dichroism induced by plasmon resonances in chiral metamaterial absorbers and bolometers Nano Lett. 18 2001–8
- [50] Hancu I M, Curto A G, Castro-López M, Kuttge M and van Hulst N F 2014 Multipolar interference for directed light emission Nano Lett. 14 166–71
- [51] Vercruysse D, Zheng X, Sonnefraud Y, Verellen N, Di Martino G, Lagae L, Vandenbosch G A, Moshchalkov V V, Maier S A and Van Dorpe P 2014 Directional fluorescence emission by individual v-antennas explained by mode expansion ACS Nano 8 8232–41
- [52] Zhou W, Dridi M, Suh J Y, Kim C H, Co D T, Wasielewski M R, Schatz G C and Odom T W 2013 Lasing action in strongly coupled plasmonic nanocavity arrays Nat. Nanotechnol. 8 506-11
- [53] Gutha R R, Sadeghi S M and Wing W J 2017 Ultrahigh refractive index sensitivity and tunable polarization switching via infrared plasmonic lattice modes Appl. Phys. Lett. 110 153103